

Fluorescent Block Copolymer Micelles That Can Self-Report on Their Assembly and Small Molecule Encapsulation

Mathew P. Robin,[†] Shani A. M. Osborne,[‡] Zoe Pikramenou,[‡] Jeffery E. Raymond,[§] and Rachel K. O'Reilly^{*,†}

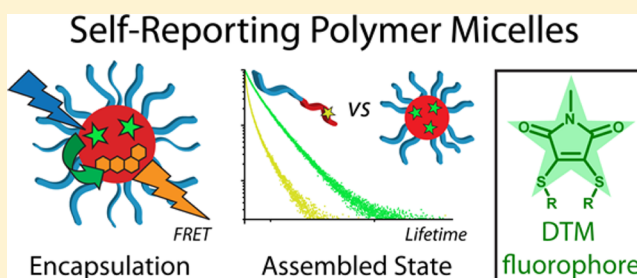
[†]Department of Chemistry, University of Warwick, Gibbet Hill Road, Coventry CV4 7AL, U.K.

[‡]School of Chemistry, The University of Birmingham, Edgbaston B15 2TT, U.K.

[§]Department of Chemistry and Laboratory for Synthetic-Biologic Interactions, Texas A&M University, College Station, Texas 77842-3012, United States

S Supporting Information

ABSTRACT: Block copolymer micelles have been prepared with a dithiomaleimide (DTM) fluorophore located in either the core or shell. Poly(triethylene glycol acrylate)-*b*-poly(*tert*-butyl acrylate) (P(TEGA)-*b*-P(*t*BA)) was synthesized by RAFT polymerization, with a DTM-functional acrylate monomer copolymerized into either the core forming P(*t*BA) block or the shell forming P(TEGA) block. Self-assembly by direct dissolution afforded spherical micelles with R_h of ca. 35 nm. Core-labeled micelles (CLMs) displayed bright emission ($\Phi_f = 17\%$) due to good protection of the fluorophore, whereas shell-labeled micelles (SLMs) had lower efficiency emission due to collisional quenching in the solvated corona. The transition from micelles to polymer unimers upon dilution could be detected by measuring the emission intensity of the solutions. For the core-labeled micelles, the fluorescence lifetime was also responsive to the supramolecular state, the lifetime being significantly longer for the micelles ($\tau_{Av,l} = 19$ ns) than for the polymer unimers ($\tau_{Av,l} = 9$ ns). The core-labeled micelles could also self-report on the presence of a fluorescent hydrophobic guest molecule (Nile Red) as a result of Förster resonance energy transfer (FRET) between the DTM fluorophore and the guest. The sensitivity of the DTM fluorophore to its environment therefore provides a simple handle to obtain detailed structural information for the labeled polymer micelles. A case will also be made for the application superiority of core-labeled micelles over shell-labeled micelles for the DTM fluorophore.



INTRODUCTION

The use of fluorescent nanoparticles as imaging agents is an increasingly important topic in the field of bioimaging.¹ The utility of fluorescence spectroscopy as a detection method for cellular imaging arises from the sensitivity of the technique, as well as the ability to discriminate based on both intensity and wavelength of emission. Fluorescent nanoparticles provide additional advantages over molecular organic fluorophores, including a reduction in fluorophore aggregation, reduced cytotoxicity, improved microenvironment inertness, better stability, and increased brightness.^{1,2} Nanoparticles derived from silica and gold, as well as quantum dots and carbon dots, have all been utilized as fluorescent imaging agents.³ However, polymer nanoparticles perhaps provide the greatest scope for versatility in particle properties and composition, such as hydrophobicity/hydrophilicity, surface chemistry, and analyte/cargo transport.⁴ Additionally, polymer nanoparticles can be designed to respond to a range of external stimuli, including temperature, pH, oxidation/reduction, biomolecules, and light.^{5,6} It is particularly desirable, in the case of fluorescent particles, if this response can be coupled to a change in emission.⁷ Encapsulation of organic dyes within polymer

nanoparticles can provide such information. For example both hydrophobic and hydrophilic dyes can be used to detect morphology changes in block copolymer (BCP) solution state self-assemblies.⁸ However, the covalent attachment, rather than physical absorption, of dye molecules to polymer nanoparticles has the advantage of greater efficiency, decreased dye leaching from the nanoparticles and eliminates uncertainties regarding the fluorophore location.⁹ Covalent labeling can be applied to a range of synthetic methodologies,¹⁰ such as nanoprecipitation¹¹ and BCP self-assembly,^{12,13} and can also be applied to the synthesis of polymer nanogels,¹⁴ conjugated polymer nanoparticles,¹⁵ and dendrimers.¹⁶ Synthetic diversity is also increased by the potential for dye incorporation using fluorescent monomers and/or initiators during polymer synthesis¹⁷ or by subsequent particle modification.¹⁸

Covalent attachment of fluorophores to BCPs has long been exploited to provide a wealth of information about the BCP self-assembled state in model systems, for example via excimer

Received: September 29, 2015

Revised: December 11, 2015

Published: January 6, 2016

emission, FRET measurements, and fluorescence lifetimes.^{19–22} More recently, this self-assembly information has also been collected *in vitro* and *in vivo*.²³ For example, the aggregation of dye labeled polymers can cause quenching processes to be enhanced or inhibited, leading upon micellization to decreased or increased emission, respectively.^{24,25} The degradation of polymer micelles derived from intrinsically fluorescent copolymers has also been observed by detecting a decrease in emission,²⁶ while the loss of mobility upon BCP micelle gelation has allowed for the glass transition temperature and critical micelle temperature to be measured by changes in emission from a covalently attached fluorophore.²⁷ Changes in the morphology of BCP assemblies can also be observed by measuring emission from fluorescent labels. For example, the swelling of micelle coronas in response to temperature and pH can be detected due to the effect on fluorophore quenching or excimer formation caused by changes in coronal hydration.^{28,29}

The controlled assembly and disassembly of BCP nanoparticles in response to a stimulus can also be detected by measuring the emission of covalently attached fluorophores. For example, Gao *et al.* have developed a series of “ultra-pH-sensitive” BCP nanoparticles, where the core block is labeled with a self-quenching fluorophore. The core block comprises of pH-responsive poly(aminomethacrylates), and protonation of this block causes a transition from hydrophobic to hydrophilic, leading to micelle disassembly.^{30–33} Micelle disassembly can therefore be detected by increased emission, while the pH range for response can be tuned from pH 4–7.4 by tailoring the poly(aminomethacrylate) allowing *in vitro* and *in vivo* detection of disassembly in the early or late endosome, for example. This approach of detecting pH triggered BCP disassembly with a self-quenching dye can also be coupled with the use of a pH-responsive fluorophore in the hydrophilic block.³⁴ In this example the pH-responsive dye emitted at a longer wavelength and was less emissive once protonated (which coincides with core block protonation and micelle disassembly), so that an enhanced signal was achieved by taking the ratio of emission at the two different wavelengths. In addition to pH, response of BCP micelles to temperature and the presence of metal ions has also been detected by fluorescence spectroscopy, using either dyes that respond to changes in aggregation or dyes whose emission changes upon binding to the metal ions.^{17,35–37}

Recent work in our group has highlighted the utility of simple fluorophores based on substituted maleimides.^{38,39} These dithiomaleimide (DTM) fluorophores were easily incorporated into superbright nanoparticles via a one-pot emulsion polymerization⁴⁰ and were also incorporated into BCP micelles whereby a change in emission enabled the detection of a micelle-to-vesicle morphology transition.⁴¹ Fluorescence lifetime imaging microscopy (FLIM) was also utilized to allow *in vitro* detection of micelle-to-unimer disassembly, as fluorophore protection from solvent collisional quenching in the assembled micelles led to longer fluorescence lifetimes, whereas the limited protection afforded to the polymer unimers resulted in a drastic reduction in fluorescence lifetime.⁴² For these self-reporting BCP micelles, the DTM fluorophore was located at the interface between the core and coronal blocks, which required the use of a DTM-labeled asymmetric dual-functional initiator for ring-opening and reversible addition–fragmentation chain-transfer (RAFT) polymerization. In the present work we aim to simplify the synthetic route to obtain self-reporting fluorescent DTM-labeled BCP micelles by utilizing a DTM-labeled acrylate

monomer to allow BCP synthesis by sequential RAFT polymerizations. The greater versatility of this synthetic approach also allowed the position of the fluorophore to be varied, and we therefore also investigated the effect of locating the fluorophore in the micelle core or corona. This approach has enabled the simplified fabrication of highly emissive fluorescent BCP micelles, whose fluorescent lifetime self-reports on the supramolecular assembled state, while the emission from the micelles can also report on the presence and location of an encapsulated organic dye.

EXPERIMENTAL SECTION

General. *tert*-Butyl acrylate (tBA) was vacuum distilled over CaH₂ prior to use and stored at 4 °C. 2,2'-Azobis(2-methylpropionitrile) (AIBN) was recrystallized twice from methanol and stored at 4 °C in the dark. Triethylene glycol monomethyl ether acrylate (TEGA),⁴³ and dithiomaleimide acrylate (DTMA),⁴⁴ were synthesized as previously reported. The RAFT agent cyanomethyldodecyl trithiocarbonate (CMDT), Nile Red (NR), and Rhodamine B (RhB) were purchased from Aldrich and used as received. 1,4-Dioxane for polymerizations (Fisher, reagent grade) was passed through a column of basic alumina immediately prior to the reaction. 1,4-Dioxane for FRET experiments (Aldrich, spectroscopy grade) was used as received. Solvents for size exclusion chromatography (Fisher, HPLC grade) were used as received. All other chemicals were purchased from Fisher or Aldrich and used as received. Water for self-assembly and spectroscopy was purified to a resistivity of 18.2 M Ω -cm using a Millipore Simplicity Ultrapure water system.

¹H and ¹³C NMR spectra were recorded on a Bruker DPX-400 spectrometer in CDCl₃ unless otherwise stated. Chemical shifts are given in ppm downfield from the internal standard tetramethylsilane. Size exclusion chromatography (SEC) measurements were conducted using a Varian 390-LC-Multi detector suite fitted with differential refractive index (DRI), UV-vis, and photodiode array (PDA) detectors. A guard column (Varian Polymer Laboratories PLGel 5 μ m, 50 mm \times 7.5 mm) and two mixed D columns (Varian Polymer Laboratories PLGel 5 μ m, 300 mm \times 7.5 mm) were used. The mobile phase was tetrahydrofuran with 2% triethylamine or dimethylformamide with NH₄BF₄ (5 mM) eluent at a flow rate of 1.0 mL/min. Data were analyzed using Cirrus v3.3 with calibration curves produced using Varian Polymer Laboratories Easi-Vials linear poly(styrene) standards (162 g mol⁻¹–240 kg mol⁻¹) or linear poly(methyl methacrylate) standards (690 g mol⁻¹–790 kg mol⁻¹). Transmission electron microscopy (TEM) imaging was performed on a Jeol 2011 200 kV LaB₆ instrument fitted with a Gatan UltraScan 1000 camera, using Agar Graphene Oxide Support Film grids.

Light Scattering. Static light scattering (SLS) and dynamic light scattering (DLS) measurements were performed on an ALV CGS3 goniometer operating at $\lambda = 632.8$ nm. The temperature of the toluene bath was regulated using a Julabo F32-ME refrigerated and heating circulator set to 20 °C. Intensity autocorrelation functions ($g_2(q,t)$) were fitted with the REPES routine using GENDIST software,⁴⁵ which performs an Inverse Laplace transformation to produce a distribution of relaxation times $A(\tau)$. An error of $\pm 10\%$ was applied to light scattering data, in accordance with previous reports.⁴⁶ Refractive index increment (dn/dc) was measured by injecting samples of a known concentration into a Shodex RI-101 refractive index detector. The response was calibrated using solutions of poly(styrene) in toluene.

An aggregation number (N_{agg}) for the particles can be calculated according to eq 1, where $M_{w,\text{polymer}}$ can be approximated by M_n (calculated by ¹H NMR spectroscopy end-group analysis) multiplied by D_M (calculated by SEC).

$$N_{\text{agg}} = \frac{M_{w,\text{particle}}}{M_{w,\text{polymer}}} \quad (1)$$

Assuming that the micelle core is completely dehydrated, it is then possible to approximate the radius of the core (R_{core}) from N_{agg} according to eq 2.⁴⁶ This equation simply relates the volume of a

sphere with radius R_{core} to the mass of the polymer core of the micelle ($M_{w,\text{core}} = M_{n,\text{core}}(\text{NMR}) \times D_{M,\text{core}}(\text{SEC})$), whose density is approximated by the bulk density of the core-forming polymer ($\rho = 1.00 \times 10^6 \text{ g m}^{-3}$ for PtBA).⁴⁷

$$\frac{4\pi\rho R_{\text{core}}^3}{3} = N_{\text{agg}} \frac{M_{w,\text{core}}}{N_A} \quad (2)$$

Core volume (V_{core}) can subsequently be calculated from R_{core} , while shell volume (V_{shell}) is calculated as the difference between total micelle volume (from R_h) and V_{core} . The approximate local concentration of the fluorophore ($[\text{DTM}]$) in the SLMs and CLMs can then be calculated according to eqs 3 and 4, respectively.

$$[\text{DTM}] = \frac{N_{\text{agg}} \text{DP}_{\text{DTMA}}}{N_A V_{\text{shell}}} \quad (3)$$

$$[\text{DTM}] = \frac{N_{\text{agg}} \text{DP}_{\text{DTMA}}}{N_A V_{\text{core}}} \quad (4)$$

Fluorescence Spectroscopy. All steady state emission, excitation, and anisotropy spectra were obtained with a Horiba FluoroMax4 with automatic polarizers and analyzed in FluorEssence (Horiba) and OriginPro 8.6 (Origin Laboratories). A long-pass emission filter ($\lambda = 360 \text{ nm}$) was used to eliminate the detection of first- and second-order Rayleigh scattering. For the emission intensity measurements the full emission spectra was integrated using the Integrate function in OriginPro and normalized by dividing by the concentration of polymer. There were negligible changes in absorption at excitation wavelength. Time-correlated single photon counting (TCSPC) was employed to obtain all fluorescence lifetime spectra. This was done with a Fluorotime 100 fluorometer and 405 nm solid state picosecond diode laser source (PicoQuant) in matched quartz 0.7 mL cells (Starna Cell). Instrument response functions (IRF) were determined from scatter signal solution of Ludox HS-40 colloidal silica (1% particles in water w/w). Analysis was performed on Fluorofit (PicoQuant). Fluorescence lifetime imaging was performed using a FLIM LSM upgrade kit for the FV1000 (PicoQuant) mounted on a FV1000 (Olympus) confocal microscope on a IX-81 inverted base (Olympus). A PlanApo N 60 \times oil lens (NA 1.42, Olympus) was used for all imaging. The FV1000 system was driven with the FV10-ASW v3.1a software platform (Olympus) with scan rates of 4 $\mu\text{s}/\text{pixel}$ at 256×256 pixels. FLIM images and spectra were collected using bins of 16 ps with a 405 nm laser (LDH-P-C-405B, PicoQuant) driven at 2.5 MHz. The fwhm for the 405 nm laser head was 60 ps, and the maximum power was 0.21 mW (attenuated by variable neutral density filters to prevent count pileup and maintain counting rates below 1% bin occupancy). SymphoTime 64 (Picoquant) software was used for collection and analysis of FLIM images and spectra. All IRF deconvolved exponential fits were performed with the 3 or 4 exponents selected for completeness of fit as determined by bootstrap χ^2 analysis in Fluorofit. Quantum yield experiments were performed on an Edinburgh Instruments FLS920 steady-state spectrometer fitted with an integrating sphere and a R928 (visible) Hamamatsu photomultiplier tube detection system. F900 spectrometer analysis software was used to record the data. Experiments were carried out in solution using 1 cm path length quartz cuvettes with four transparent polished faces.

Polymer Synthesis. *P(tBA)* (1). A solution of CMDT (0.282 g, 887 μmol), tBA (5.00 g, 39.0 mmol), and AIBN (14.6 mg, 88.7 μmol) in 1,4-dioxane (5.66 mL) was added to a polymerization ampule. The solution was degassed by three freeze–pump–thaw cycles and sealed under N_2 . The reaction was stirred at 65 $^\circ\text{C}$ for 2 h and then quenched by rapid cooling and exposure to air. The product was purified by repeated precipitation into ice-cold methanol/ H_2O (9/1, v/v) and isolated as a yellow glassy solid. $\text{DP}_{\text{tBA}}(\text{NMR}) = 44$, $M_n(\text{NMR}) = 6.0 \text{ kg mol}^{-1}$, and $D_M(\text{SEC}) = 1.08$.

P(tBA-co-DTMA) (2). A solution of CMDT (40.0 mg, 126 μmol), tBA (0.807 g, 6.30 mmol), DTMA (81.2 mg, 189 μmol), and AIBN (2.07 mg, 12.6 μmol) in 1,4-dioxane (0.914 mL) was added to a

polymerization ampule. The solution was degassed by three freeze–pump–thaw cycles and sealed under N_2 . The reaction was stirred at 65 $^\circ\text{C}$ for 5 h and then quenched by rapid cooling and exposure to air. The product was purified by repeated precipitation into ice-cold methanol/ H_2O (9/1, v/v) and isolated as a fluorescent yellow glassy solid. $\text{DP}_{\text{tBA}}(\text{NMR}) = 36$, $\text{DP}_{\text{DTMA}}(\text{NMR}) = 1.1$, $M_n(\text{NMR}) = 5.4 \text{ kg mol}^{-1}$, and $D_M(\text{SEC}) = 1.13$.

P(TEGA)-b-P(tBA) Block Copolymer (3). A solution of 1 (0.150 g, 25.2 μmol), TEGA (0.878 g, 4.02 mmol), and AIBN (0.41 mg, 2.5 μmol) in 1,4-dioxane (2.37 mL) was added to a polymerization ampule. The solution was degassed by three freeze–pump–thaw cycles and sealed under N_2 . The reaction was stirred at 65 $^\circ\text{C}$ for 4.5 h and then quenched by rapid cooling and exposure to air. H_2O (10 mL) was added, and the solution purified by exhaustive dialysis (MWCO 3.5 kg mol^{-1}) against distilled water. The product was obtained as a yellow waxy solid by lyophilization. $\text{DP}_{\text{TEGA}}(\text{NMR}) = 120$, $M_n(\text{NMR}) = 31.3 \text{ kg mol}^{-1}$, and $D_M(\text{SEC}) = 1.38$.

P(TEGA-co-DTMA)-b-P(tBA) Block Copolymer (4). A solution of 1 (0.150 g, 25.2 μmol), TEGA (1.10 g, 5.03 mmol), DTMA (16.2 mg, 37.7 μmol), and AIBN (0.41 mg, 2.5 μmol) in 1,4-dioxane (2.96 mL) was added to a polymerization ampule. The solution was degassed by three freeze–pump–thaw cycles and sealed under N_2 . The reaction was stirred at 65 $^\circ\text{C}$ for 5 h and then quenched by rapid cooling and exposure to air. 1,4-Dioxane (2 mL) was added, and the solution precipitated into ice-cold hexane (200 mL \times 2). The crude product was redissolved in 1,4-dioxane/ H_2O (1/2, v/v) and purified by exhaustive dialysis (MWCO 3.5 kg mol^{-1}) against distilled water. The product was obtained as a fluorescent yellow waxy solid by lyophilization. $\text{DP}_{\text{TEGA}}(\text{NMR}) = 140$, $\text{DP}_{\text{DTMA}}(\text{NMR}) = 1.1$, $M_n(\text{NMR}) = 37.7 \text{ kg mol}^{-1}$, and $D_M(\text{SEC}) = 1.35$.

P(TEGA)-b-P(tBA-co-DTMA) Block Copolymer (5). A solution of 2 (0.130 g, 24.3 μmol), TEGA (1.06 g, 4.86 mmol), and AIBN (0.40 mg, 2.4 μmol) in 1,4-dioxane (2.86 mL) was added to a polymerization ampule. The solution was degassed by three freeze–pump–thaw cycles and sealed under N_2 . The reaction was stirred at 65 $^\circ\text{C}$ for 3.5 h and then quenched by rapid cooling and exposure to air. H_2O (10 mL) was added, and the solution purified by exhaustive dialysis (MWCO 3.5 kg mol^{-1}) against distilled water. The product was obtained as a fluorescent yellow waxy solid by lyophilization. $\text{DP}_{\text{TEGA}}(\text{NMR}) = 130$, $M_n(\text{NMR}) = 33.1 \text{ kg mol}^{-1}$, and $D_M(\text{SEC}) = 1.38$.

Block Copolymer Self-Assembly. Nonlabeled micelles (NLMs), shell-labeled micelles (SLMs), and core-labeled micelles (CLMs) were assembled by direct dissolution of 3, 4, and 5, respectively, in water (18.2 $\text{M}\Omega\text{-cm}$) at a concentration of 1 g/L. In order to fully disperse the particles the solutions were stirred at 60 $^\circ\text{C}$ for 3 h and then sonicated until completely transparent.

FRET Experiments. For the composition of solutions for FRET experiments shown in Figure 8, see Table S1 in the Supporting Information. General procedures were as follows.

Mixing CLMs and NR. A stock solution of NR in 1,4-dioxane was prepared at a concentration of 0.1 mM. A 1 g/L solution of CLMs (82.8 μL) was diluted with water (2417 μL) to give $[\text{DTM}] = 1 \mu\text{M}$. To this micelle solution was added 2.5 μL of the NR stock solution to give a final $[\text{NR}] = 0.1 \mu\text{M}$. The solution was mixed with a vortex mixer for 1 s, and the emission was monitored by fluorescence spectroscopy.

Mixing NLMs and NR. The procedure above (CLMs and NR) was repeated for solutions of NLMs. In this case a 1 g/L solution of NLMs (79.9 μL) was diluted with water (2420 μL) to give $[\text{3}] = 1 \mu\text{M}$.

Mixing CLMs and RhB. The procedure above (CLMs and NR) was repeated for solutions of CLMs and RhB. In this case a stock solution of RhB in water was prepared at a concentration of 0.1 mM.

RESULTS AND DISCUSSION

Block Copolymer Synthesis. In order to synthesize BCP micelles with DTM fluorophores in the shell or core, it was necessary to synthesize two different BCPs. Shell-labeled micelles (SLMs) require a BCP with the DTM fluorophore in the hydrophilic block, while core-labeled micelles require a

BCP with the DTM fluorophore in the hydrophobic block (Figure 1).

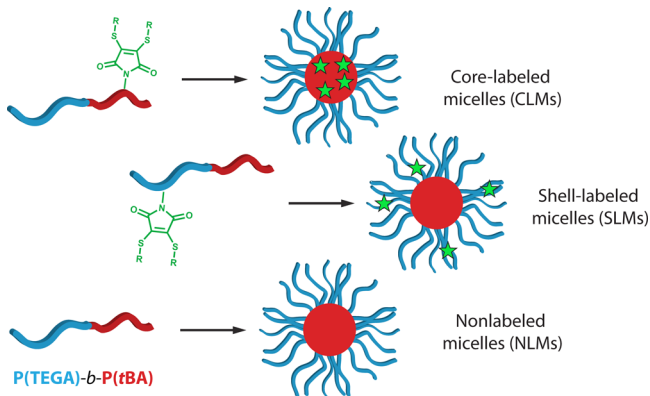


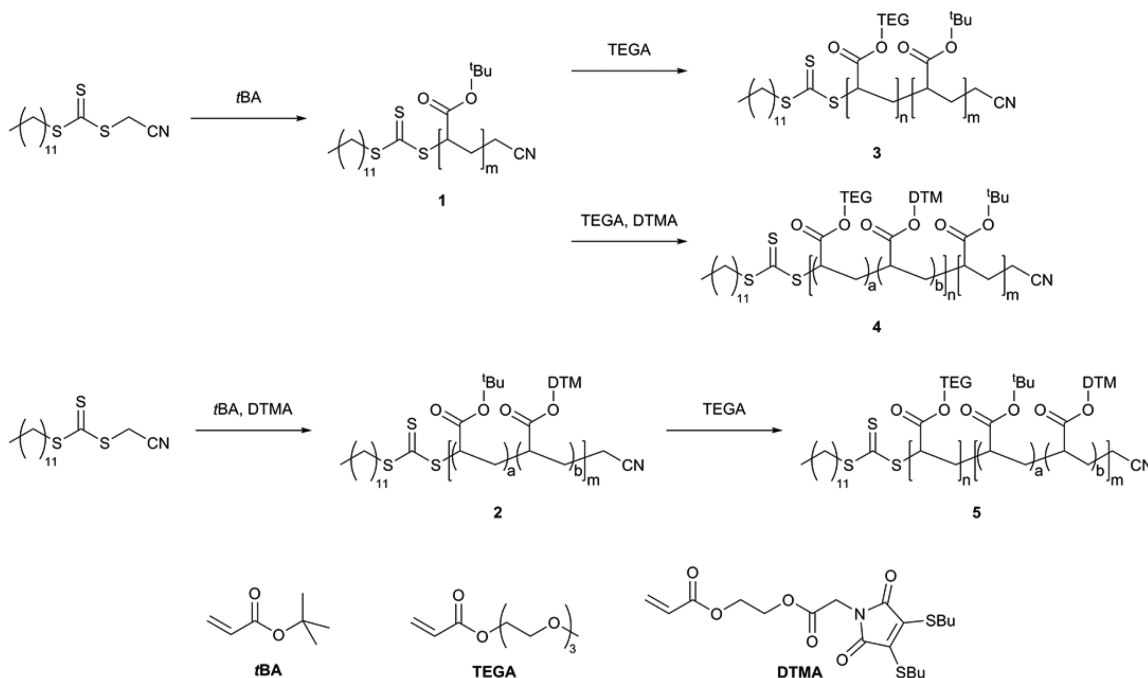
Figure 1. Schematic representation of the route to shell-labeled micelles (SLMs) and core-labeled micelles (CLMs) containing the DTM fluorophore and the route to nonlabeled micelles (NLMs).

The BCPs used to form the labeled micelles were based on poly(triethylene glycol acrylate)-*b*-poly(*tert*-butyl acrylate), P(TEGA)-*b*-P(*t*BA), with an average of approximately one repeat unit per chain of dithiomaleimide acrylate (DTMA)⁴⁴ copolymerized into either the P(TEGA) shell-forming block or P(*t*BA) core-forming block, as shown in Scheme 1. A nonfunctional P(TEGA)-*b*-P(*t*BA) was also synthesized to allow self-assembly of nonlabeled micelles (NLMs) for comparison. The DTM fluorophore is ideally suited to this variable approach to BCP labeling, as the small size and intermediate polarity of the fluorophore mean that it is simply incorporated into both hydrophobic and hydrophilic polymers.⁴⁴

The hydrophobic core blocks (**1** and **2**) were synthesized first by RAFT polymerization of *t*BA, using the commercially available RAFT agent cyanomethyl dodecyl trithiocarbonate, with AIBN (0.1 equiv with respect to RAFT agent) as radical initiator, as a solution in 1,4-dioxane at 65 °C. The nonlabeled core block **1** (to be used to form shell- and nonlabeled micelles) consisted of a P(*t*BA) homopolymer, while for the labeled core block **2** (to be used to form core-labeled micelles) a copolymer of *t*BA with DTMA was synthesized. For **2**, an average DP of 1 was targeted for DTMA to give incorporation of a single fluorophore per chain. ¹H NMR spectroscopy indicated that for the nonlabeled homopolymer (**1**) DP_{*t*BA} = 44, while for the labeled copolymer (**2**) DP_{*t*BA} = 36 and DP_{DTMA} = 1.1. For both **1** and **2** the presence of the trithiocarbonate end-group was confirmed by characteristic resonances of the dodecyl chain (both H1 and H4 in Figures S1 and S2). SEC analysis of **1** and **2** indicated a good control over molecular weight ($D_M = 1.08$ and 1.13, respectively), with trithiocarbonate retention indicated by polymer absorption at 309 nm (Figure 2 and Table 1). Additionally, SEC analysis of **2** using a photodiode array detector showed incorporation of the DTM chromophore, with the polymer peak having the characteristic DTM absorption at *ca.* 400 nm (Figure S3).

BCPs were produced by the chain extension of the macro-RAFT agents **1** and **2** according to Scheme 1. Chain extension of **1** with TEGA resulted in the nonlabeled BCP **3**, the precursor to the nonlabeled micelles, while chain extension of **1** with TEGA and DTMA (targeting an average DP of 1 for DTMA to give incorporation of a single fluorophore per chain) resulted in **4**, the precursor to shell-labeled micelles containing the DTM fluorophore in the corona forming TEGA block. ¹H NMR spectroscopy indicated that **3** had DP_{TEGA} = 120, while **4** had DP_{TEGA} = 140 and DP_{DTMA} = 1.1 (Figures S4 and S5), giving hydrophobic weight fractions (f_C) of 18% and 15% for **3**

Scheme 1. Synthesis of a Nonlabeled P(TEGA)-*b*-P(*t*BA) Block Copolymer (**3**), Block Copolymers with a Dithiomaleimide Label in the Shell-Forming Block (**4**), and the Core-Forming Block (**5**)^a



^aConditions for all polymerizations: AIBN (0.1 equiv with respect to RAFT agent), 1,4-dioxane, 65 °C.

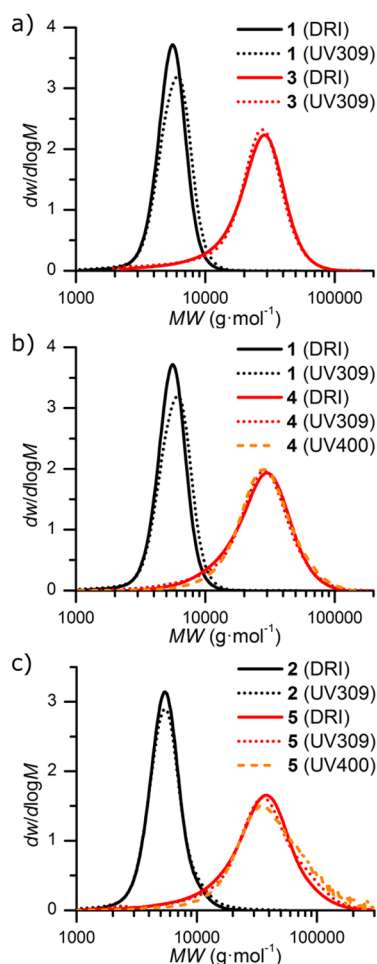


Figure 2. Molecular weight distributions obtained by SEC using differential refractive index (DRI) and UV ($\lambda_{\text{abs}} = 309$ or 400 nm) detectors for (a) P(*t*BA) (1) and P(TEGA)-*b*-P(*t*BA) (3), (b) P(*t*BA) (1) and P(TEGA-*co*-DTMA)-*b*-P(*t*BA) (4), and (c) P(*t*BA-*co*-DTMA) (2) and P(TEGA)-*b*-P(*t*BA-*co*-DTMA) (5).

Table 1. Characterization Data for Polymers 1–5

polymer	M_n^a (kg mol^{-1})	M_n^b (kg mol^{-1})	D_M^b
1 P(<i>t</i> BA) ₄₄	6.0	5.2	1.08
2 P(<i>t</i> BA ₃₆ - <i>co</i> -DTMA _{1,1})	5.4	5.1	1.13
3 P(TEGA) ₁₂₀ - <i>b</i> -P(<i>t</i> BA) ₄₄	31.3	20.1	1.38
4 P(TEGA) ₁₄₀ - <i>co</i> -DTMA _{1,1} - <i>b</i> -P(<i>t</i> BA) ₄₄	37.7	21.9	1.35
5 P(TEGA) ₁₃₀ - <i>b</i> -P(<i>t</i> BA ₃₆ - <i>co</i> -DTMA _{1,1})	33.1	26.7	1.38

^aCalculated by ¹H NMR spectroscopy end-group analysis. ^bMeasured by SEC (1, 2: THF eluent and PS calibration; 3, 4, 5: DMF eluent and PMMA calibration).

and 4, respectively, which would likely favor the formation of star-like spherical micelles upon aqueous self-assembly.⁴⁸ Chain extension of 2 with TEGA resulted in BCP 5 with a labeled core forming block (the precursor to core-labeled micelles). ¹H NMR spectroscopy indicated that 5 had $DP_{\text{TEGA}} = 130$ (Figure S6), corresponding to a hydrophobic weight fraction (f_c) of 16%. In all cases SEC indicated good blocking efficiency, with molecular weight distributions obtained from both differential refractive index and UV ($\lambda_{\text{abs}} = 309$ nm) detectors showing consumption of the macro-RAFT agents 1 and 2, with a

reasonable control over molecular weight ($D_M = 1.35$ – 1.38 for 3–5). By monitoring absorption at 400 nm (absorption due to the DTM chromophore), incorporation of DTMA into the corona forming block of 4 was also confirmed (Figure 2).

Block Copolymer Self-Assembly. The amphiphilic BCPs 3–5 were assembled by direct dissolution in water ($18.2 \text{ M}\Omega\text{-cm}$) at a concentration of 1 g/L. In order to fully disperse the particles, the solutions were stirred at 60 °C for 3 h and then sonicated until completely transparent. Self-assembled solutions of 3–5 were analyzed by multiangle laser light scattering using a goniometer allowing simultaneous dynamic and static light scattering (DLS and SLS) measurements (see Table 2 and Figure S7). Particle hydrodynamic radius (R_h) was

Table 2. DLS/SLS Characterization Data for Micelles Obtained by the Solution Self-Assembly of BCPs 3–5

	NLMs	SLMs	CLMs
BCP	3	4	5
f_c (%)	18	15	16
R_h (nm)	36	34	36
N_{agg}	150	40	110
[DTM] (mM)		0.40	180

obtained directly from DLS measurements and in all cases was approximately equivalent with $R_h = 34$ – 36 nm (Figure 3). Measurement of particle M_w by SLS allowed for the calculation of aggregation number (N_{agg}), which was found to vary between the systems (Table 2). The trend of increasing N_{agg} with f_c could be explained by considering that polymer unimers with higher f_c (greater hydrophobic character) are less stable in aqueous solution and therefore have a lower energy barrier for insertion. Despite this variation in N_{agg} , the structural similarity of the DTM-labeled micelles (prepared from 4 and 5) to the nonlabeled micelles (prepared from 3) indicates that incorporation of the DTM label has not had a detrimental effect on the BCP self-assembly. From R_h and N_{agg} it is also possible to estimate the micelle core and shell volumes (V_{core} and V_{shell}),^{46,49} and hence the local concentration of DTM fluorophores within the micelles ([DTM]) could be calculated (see Experimental Section for details). These calculations revealed that despite using the same ratio of dye for labeling the BCPs 4 and 5 (*ca.* 1 equiv per chain), two very different local environments can be created: a *ca.* 400-fold decrease in local concentration is obtained by locating the DTM in the shell (SLMs) compared to locating the DTM in the core (CLMs).

Micelle solutions were imaged by dry state transmission electron microscopy (TEM) using graphene oxide support TEM grids in order to examine micelle morphology.^{50,51} As shown in Figure 3, particles provided a circular projection when dried to a graphene oxide surface, suggesting they had a spherical morphology. In line with previous observations,⁵⁰ only the P(*t*BA) micelle cores provided sufficient contrast to be visualized by TEM, with core diameters in reasonable agreement with those obtained by light scattering.

Steady State Fluorescence Spectroscopy. The steady state emission and excitation spectra for solutions of labeled micelles were found to be very similar to that of analogous small molecule DTMs.^{38,42,44} A 2D excitation–emission spectrum for the core-labeled micelles is shown in Figure 4a, with excitation maxima occurring at 267 and 407 nm, with the corresponding emission maximum of 510 nm (Figure 4b). The fluorescence quantum yield (Φ_f) for the core-labeled micelles

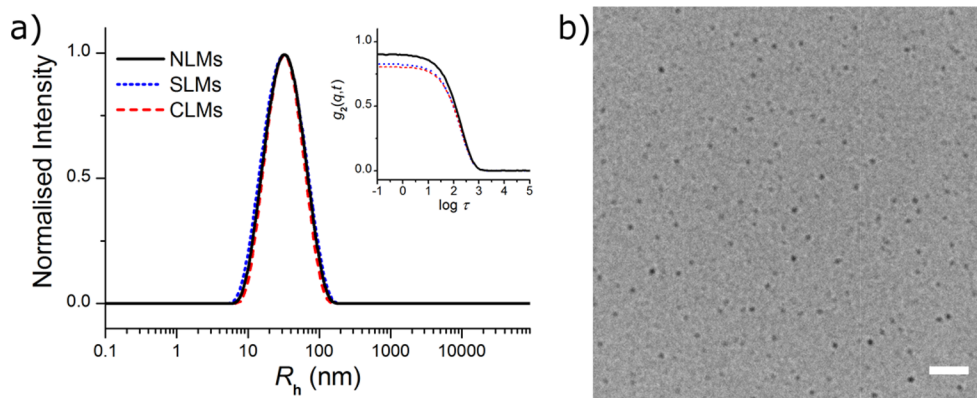


Figure 3. (a) Size distribution obtained by DLS (detection angle of 90°) for a solution of NLMs, SLMs, and CLMs at 1 g/L and the corresponding autocorrelation functions (inset). (b) SLMs imaged by TEM on a graphene oxide support. Scale bar = 100 nm.

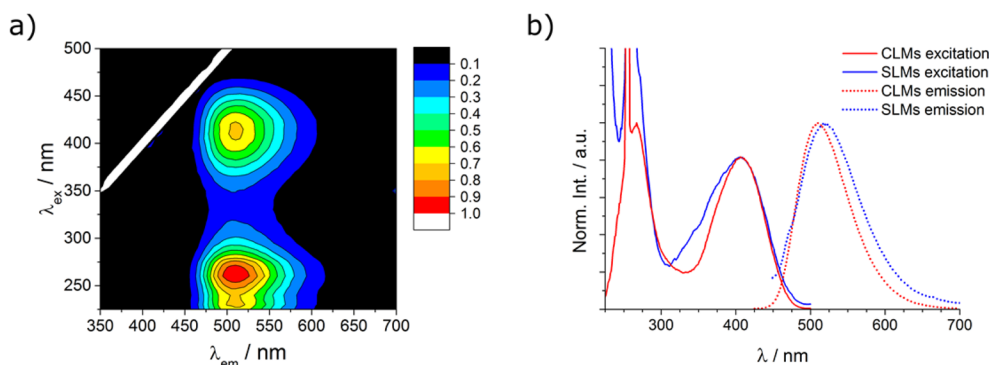


Figure 4. (a) 2D excitation–emission spectra with a 5 nm step for an aqueous solution of core-labeled micelles. (b) Excitation and emission spectra of aqueous solutions of core- and shell-labeled micelles.

was measured using an integrating sphere to give an absolute value of $17 \pm 2\%$. Excitation and emission spectra were also recorded for the shell-labeled micelles, which showed similar excitation and emission. However, a red-shift in the emission maximum ($\lambda_{em,max}$) to 520 nm was observed with a drastic reduction in Φ_f to $<1\%$, as compared to the core-labeled micelles. The drastic reduction of Φ_f and bathochromic shift of emission indicates the different environment of the chromophore, which is consistent with collisional (solvent) quenching in the more polar environment of the solvated micelle shell. These results are in agreement with previous work using small molecule DTM fluorophores which show both bathochromic shifts and reductions in Φ_f upon increasing solvent polarity; for example, dithiobutanemaleimide has $\lambda_{em,max} = 486$ nm and $\Phi_f = 28\%$ in cyclohexane, whereas in methanol $\lambda_{em,max} = 546$ nm and $\Phi_f < 1\%$.³⁹ While the possibility of ordered, coherent effects cannot be overtly discounted, we have seen nothing to indicate aggregation-induced emission,⁵² a process which is typically reserved for discussions of neat or chromophore-rich, highly ordered systems with J-type emission or H-type systems that interconvert to J-type emission.

Emission intensity was measured over a range of concentrations for aqueous solutions of the polymers 4 and 5, whereby the integrated emission was calculated for the whole spectrum and these values normalized by the concentration of polymer chains in solution (Figure 5). For both polymers a relatively flat emission intensity over 3 orders of magnitude in concentration was observed, corresponding to the micellar state (shell-labeled micelles for 4 and core-labeled micelles for 5). Deviation from the flat emission intensity occurred at $c \leq 1 \times$

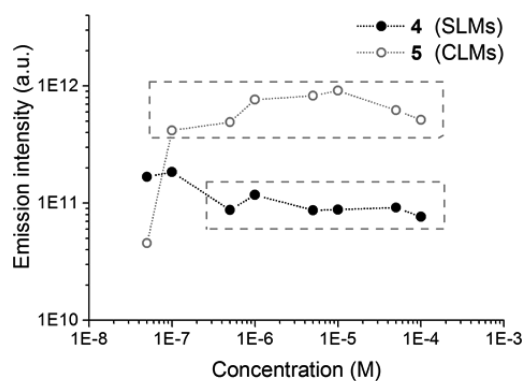


Figure 5. Emission intensity (normalized to polymer chain concentration) with respect to concentration for polymers 4 and 5.

10^{-7} M for 4 and $c \leq 5 \times 10^{-8}$ M for 5 and was assigned to a transition from micelles to solvated polymer unimers upon decreasing concentration.⁴² For polymer 4 the DTM fluorophore is already solvated by water in the micelle shell, so the transition from micelles to unimers leads to an increase in emission intensity due to increased protection from solvent interactions with the presence of the hydrophobic core block in the unimer coil. However, for polymer 5 the DTM fluorophore is protected from the surrounding solvent due to its location in the micelle core. Therefore, upon transition to the polymer unimer state an increase in solvation occurs, leading to dye–solvent quenching and a corresponding decrease in emission intensity. In both cases, the emission intensity self-reports on

the supramolecular state of the polymer allowing a convenient way to determine the critical micelle concentrations (CMCs), which correspond to 3.8 and 1.7 mg/L for shell- and core-labeled micelles, respectively. The higher CMC of the shell-labeled micelles relative to the core-labeled micelles is in agreement with the shell-labeled micelles possessing a lower N_{agg} —both phenomena being explained by a greater solubility of unimers of polymer 4 relative to 5 due to 4 having a lower f_C . Within the micellar region emission anisotropy (r) for both 4 and 5 was found to be 0.29 ± 0.01 and 0.19 ± 0.01 , respectively, further confirming that the emissive DTM fluorophore was incorporated into a macromolecular structure, as analogous small molecule DTM dyes have $r \text{ ca. } 0$ in solution.^{40,42} It is valuable to observe that the total increase in emission intensity for polymer 4 is not as severe as the decrease in the emission intensity observed in polymer 5 on transition to the unimer state from the micellar state. Additionally, it is interesting to note that the higher dye density ($[DTM]$) within the core block of the core-labeled micelles does not result in overt quenching. This is important in terms of application, where total change in intensity for a given species will be critical and where the initial species (micelle) should be as bright as possible, and points to a core-labeled system being more viable than a corona-labeled one.

Time-Correlated Single Photon Counting and Fluorescence Lifetime Imaging Microscopy. Fluorescence lifetime was measured for aqueous solutions of polymers 4 and 5 using time-correlated single photon counting. Samples were excited with a pulsed 405 nm diode laser (60 ps full width at half-maximum), and the resultant emission decays were modeled as a sum of exponential decays after deconvolution with the instrument response function. Decay spectra are shown in Figure 6, with the average lifetimes and lifetime components listed in Table 3. For both 4 and 5 spectra were recorded for an aqueous solution at 5×10^{-5} M corresponding to the micellar regime (shell- and core-labeled micelles) and an aqueous solution at 5×10^{-8} M corresponding to polymer unimers (below the CMC). A dehydrated thin film was also prepared by drying a drop of micelle solution to a glass slide, with the spectra collected by fluorescence lifetime imaging microscopy, where the intensity decay was calculated by summation of the decays for each pixel in the image (Figure S8).

The fluorescence lifetime decay spectra clearly exhibit two important features. The first is that the shell-labeled micelles formed from 4 have a significantly faster decay than the core-labeled micelles formed from 5, with intensity-averaged lifetimes of the excited state ($\tau_{\text{Av,I}}$) of 7.0 ± 0.1 and 18.8 ± 0.3 ns, respectively. This is as a result of a near ultrafast lifetime component with significant amplitude for shell-labeled micelles ($\tau_1 = 0.40 \pm 0.06$ ns, $A_1 = 0.71$), which is assigned to excited state annihilation by solvent collision and can be interpreted as the result of poor fluorophore protection. In contrast, the major lifetime component for the core-labeled micelles is $\tau_2 = 17.5 \pm 0.1$ ns, with amplitude $A_2 = 0.96$. For the core-labeled micelles the dye is located within the dehydrated core and is therefore encapsulated within the supramolecular structure, whereas for the shell-labeled micelles location of the dye within the solvated corona provides poor protection to the DTM fluorophore from solvent quenching. This interpretation is supported by the decay spectrum of unimers of 4, which also have $\tau_{\text{Av,I}} = 7.0 \pm 0.1$ ns (near ultrafast lifetime component $\tau_1 = 0.32 \pm 0.06$ ns, $A_1 = 0.72$), indicating that shell-labeled micelle formation does

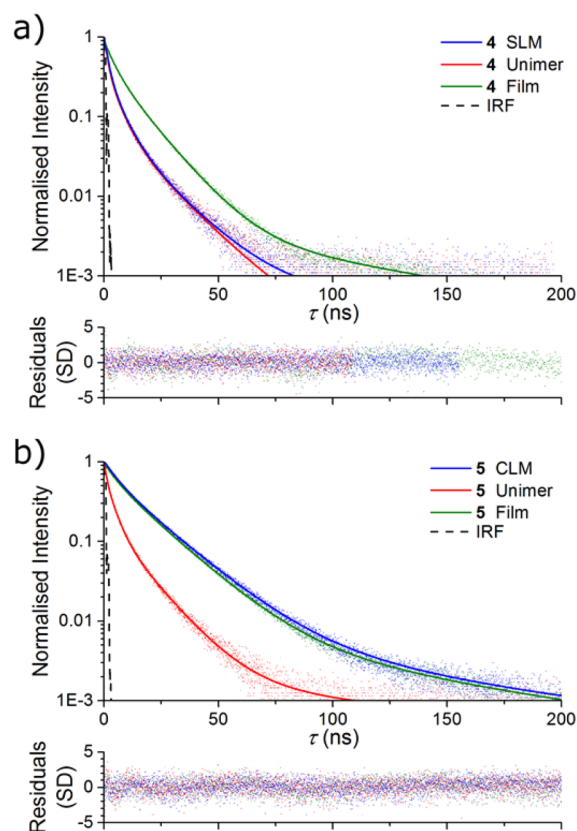


Figure 6. Fluorescence lifetime decay spectra (points), with fitting (lines), residuals (bottom), and instrument response function (IRF), for aqueous solutions of (a) 4 and (b) 5.

not change the local environment for the DTM, whereas an increase in $\tau_{\text{Av,I}}$ to 14.8 ± 0.3 ns for the dehydrated film of 4 gives a closer representation to the intrinsic lifetime for polymer 4. These results are in agreement with the observation of a lower Φ_f for the shell-labeled micelles compared to the core-labeled micelles and further emphasize that the optimum location for the DTM dye to obtain the greatest emission is within the micelle core.

The second important feature that the decay spectra highlight is the ability to discriminate the micellar state of 5 from measurements of fluorescence lifetime. A relatively long lifetime was observed for 5 in the micellar state ($\tau_{\text{Av,I}} = 18.8 \pm 0.3$ ns), whereas the unimer state showed a significant decrease to $\tau_{\text{Av,I}} = 9.2 \pm 0.2$ ns, due to a near ultrafast (solvent collision) component to the decay ($\tau_1 = 0.56 \pm 0.06$ ns, $A_1 = 0.60$). Again this interpretation was supported by fluorescence lifetime imaging microscopy measurements of a dehydrated film of micelles, which had the same decay as the micelle solution ($\tau_{\text{Av,I}} = 18.5 \pm 0.2$ ns), indicating that the core of the core-labeled micelles is largely solvent free. We have previously shown with a related interface-labeled system that this ability to discriminate between micelles and unimers simply by measuring fluorescence lifetime could be translated to *in vitro* imaging, such that micelles and unimers could be located within discrete areas of rat hippocampal tissue.⁴² As the micelle-to-unimer transition is widely exploited as a trigger for controlled drug delivery from polymer nanoparticles,²³ we expect that this feature of the core-labeled DTM micelles would provide a simple method to identify such controlled release *in vitro*.

Table 3. Kinetic Data for Solution State Fluorescence Emission Decay Spectra

	τ_1 (ns)	A_1	τ_2 (ns)	A_2	τ_3 (ns)	A_3	τ_4 (ns)	A_4	$\tau_{Av,I}$ (ns)
4 SLMs	0.40 ± 0.06	0.71	1.8 ± 0.1	0.01	5.4 ± 0.1	0.23	15.9 ± 0.3	0.05	7.0 ± 0.1
4 polymer unimers	0.32 ± 0.06	0.72	1.5 ± 0.1	0.01	5.0 ± 0.1	0.22	15.5 ± 0.2	0.05	7.0 ± 0.1
5 CLMs	5.5 ± 0.2	0.02	17.5 ± 0.1	0.96	73.7 ± 2.7	0.02			18.8 ± 0.3
5 polymer unimers	0.56 ± 0.06	0.60	3.4 ± 0.1	0.31	12.5 ± 0.2	0.09			9.2 ± 0.2

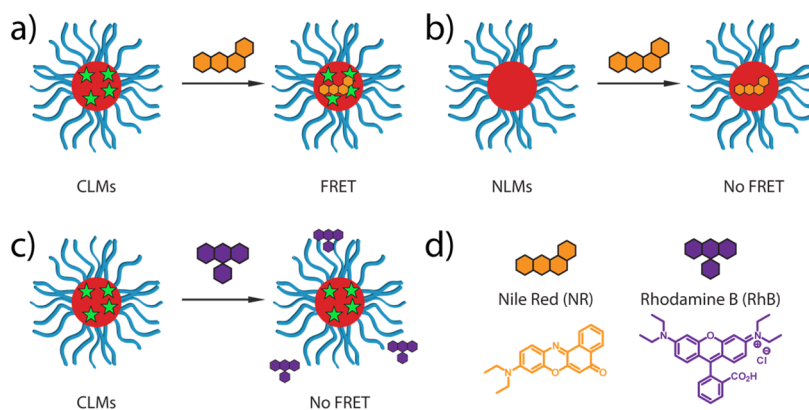


Figure 7. (a–c) Schematic representation of interaction between micelles and fluorescent dyes Nile Red (NR) and Rhodamine B (RhB). (d) Structures of Nile Red and Rhodamine B.

Monitoring CLM Loading by FRET. FRET describes a phenomenon whereby two fluorophores can interact when in close proximity to one another. Energy transfer occurs between a donor molecule in the excited state and an acceptor molecule, provided there is sufficient spectral overlap between donor emission and acceptor excitation and that the two molecules are positioned within the necessary Förster distance. The result is emission from the acceptor fluorophore upon excitation of the donor fluorophore, according to their respective excitation and emission wavelengths. Monitoring the FRET process for fluorescently labeled micelles has been exploited to measure CMCs,^{20,53} to identify morphology response to stimuli,⁵⁴ and to follow the uptake and release of fluorescent payloads.⁵⁵

Because of the interest surrounding the use of nanoparticles as delivery agents,⁵⁶ we sought to investigate whether the uptake of model compounds by the core-labeled micelles could be identified using FRET. The DTM fluorophore was designated as the FRET donor due to its broad excitation spectra and to also ensure that all emission originated from a labeled micelle. Two FRET acceptor molecules whose excitation spectra overlapped with the DTM emission were chosen as probes for interaction with, and uptake into, the core-labeled micelles: Nile Red (NR) as a hydrophobic guest expected to partition to the micelle core and Rhodamine B (RhB) as a hydrophilic guest expected to partition to the aqueous solution or the solvated micelle shell (Figure 7). To reduce the background fluorescence (i.e., non-FRET emission) from the probes, a 10-fold excess in total DTM concentration was used relative to Nile Red and Rhodamine B concentration, while all dyes were present at concentrations corresponding to an absorbance <0.1 to negate inner filter effects.

To study uptake of the hydrophobic dye, a solution of Nile Red in 1,4-dioxane ($2.5 \mu\text{L}$, 0.1 mM) was added to a solution of core-labeled micelles (2.5 mL) with $[\text{DTM}] = 1 \mu\text{M}$, to give a final $[\text{Nile Red}] = 0.1 \mu\text{M}$. Emission spectra were recorded for the solution with an excitation wavelength of 422 nm , corresponding to the excitation maximum of the DTM donor. Quenching of the DTM emission at 515 nm was

observed, with a corresponding enhancement of Nile Red emission at 610 nm (Figures 7a and 8a). Quenching and enhancement occurs within 10 s (the time of the first measurement, see Figure S9), at which time equilibrium has been reached with no further change after 60 min . These results demonstrate that FRET occurs between donor (DTM) and acceptor (Nile Red), indicating the proximity of the two fluorescent species. As FRET is extinguished beyond the Förster distance (typically $<4 \text{ nm}$), FRET between DTM and Nile Red corresponds to the presence of Nile Red within the core of the core-labeled micelles. As a control, the protocol of Nile Red addition was repeated for a solution of nonlabeled micelles where the polymer concentration was maintained with respect to the core-labeled micelles (Figures 7b and 8b). In this case an increase in emission at 610 nm was observed, as it is well-known that Nile Red emission is quenched in water and subsequently restored upon partition to a more hydrophobic environment. However, the detectable change in emission that results from this “background” increase in Nile Red brightness upon partition was $2.5\times$ lower than the combined partition and FRET effect observed for the core-labeled micelles. In addition, a greater ambiguity is associated with the interpretation of changes in Nile Red emission on its own, as these variations result from any change in environment polarity.

Finally, the FRET experiment was repeated for the core-labeled micelles using the hydrophilic dye Rhodamine B (Figures 7c and 8c), which was added to the solution of core-labeled micelles as a solution in water ($2.5 \mu\text{L}$, 0.1 mM) to give a final $[\text{Rhodamine B}] = 0.1 \mu\text{M}$. In this case no change in the intensity of emission at 515 nm was observed (DTM emission was not quenched), while the intensity of emission at 615 nm was accounted for by a summation of the emission from core-labeled micelles ($t = 0$) and a $0.1 \mu\text{M}$ Rhodamine B solution in water (Rhodamine B emission was not enhanced). This experiment therefore shows that FRET does not occur between the DTM fluorophore in core-labeled micelles and Rhodamine B, indicating that Rhodamine B does not partition to the core of the core-labeled micelles. Collectively these FRET experi-

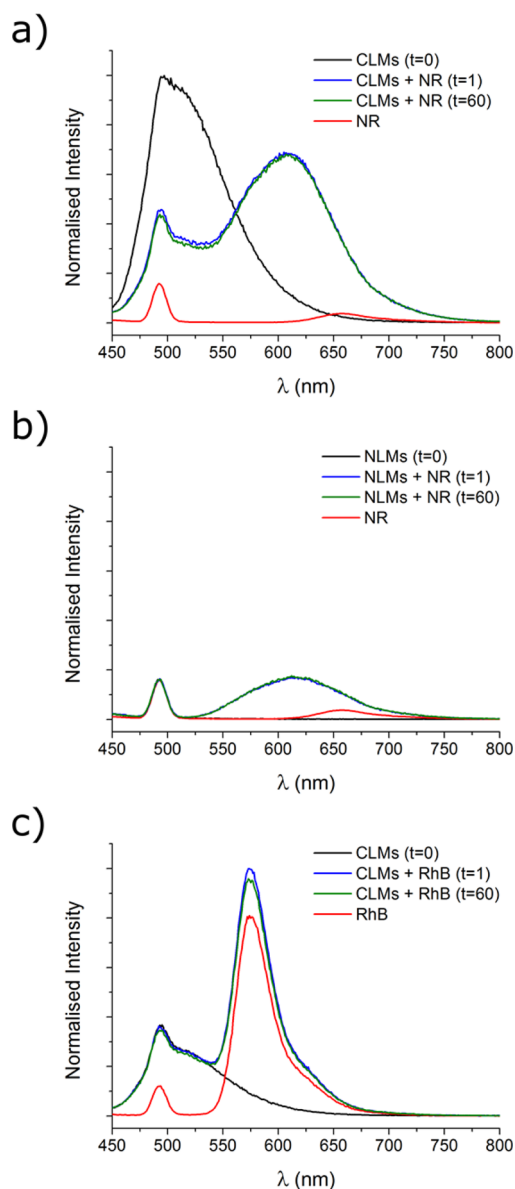


Figure 8. (a) Emission spectra of CLMs at $t = 0$, CLMs at 1 min ($t = 1$) and 60 min ($t = 60$) after addition of Nile Red (NR), and NR in water (0.1% 1,4-dioxane). (b) Emission spectra of NLMs at $t = 0$, NLMs at 1 min ($t = 1$) and 60 min ($t = 60$) after addition of NR, and NR in water (0.1% 1,4-dioxane). (c) Emission spectra of CLMs at $t = 0$, CLMs at 1 min ($t = 1$) and 60 min ($t = 60$) after addition of Rhodamine B (RhB), and RhB in water. $\lambda_{\text{ex}} = 422$ nm in all cases, and peaks at 495 nm correspond to the Raman scattering of water.

ments demonstrate that the incorporation of the DTM dye in the core-labeled micelles allows the micelles to report on the presence (Nile Red) or absence (Rhodamine B) of a cargo molecule within the micelle core via a simple measure of emission. Furthermore, although too fast in this example, measuring the rate for FRET could provide details of the kinetics of cargo encapsulation and release, as has been shown previously for core cross-linked polymer nanoparticles.⁵⁷ Taken in conjunction with the steady state and time-resolved fluorescence data, this final finding points to DTM core labeling being superior to coronal labeling for all of the most major considerations in nanocontrast/nanotherapeutic systems: it can be seen (bright), it can report on the supramolecular

state (changes in emissive character), and it can signal with regards to loading/unloading (FRET).

CONCLUSIONS

Poly(triethylene glycol acrylate)-*b*-poly(*tert*-butyl acrylate) BCP micelles have been synthesized with a fluorescent DTM group incorporated into the micelle core or shell. The advantages of using DTM chemistry are the small size and intermediate polarity of this fluorophore as well as its excellent compatibility with BCP synthesis and self-assembly and its proven applicability to tissue imaging. It was found locating the DTM fluorophore in the micelle core resulted in greater emission ($\Phi_f = 17\%$) and a longer fluorescence lifetime ($\tau_{\text{Av,I}} = 19$ ns), when compared to locating the fluorophore in the shell ($\Phi_f < 1\%$, $\tau_{\text{Av,I}} = 7$ ns), as a result of better protection of the fluorophore in the core from solvent collisional quenching. For both shell and core-labeled micelles it was possible to measure the onset of aggregation (with respect to concentration) by measuring the emission intensity. The transition from micelle-to-unimer could also be detected for the core-labeled micelles by fluorescence lifetime spectroscopy since the polymer unimers have a significantly shorter lifetime ($\tau_{\text{Av,I}} = 9$ ns). Following our previous work,⁴² we believe that the core-labeled micelles' ability to self-report on their supramolecular state would allow *in vitro* discrimination between assembled and disassembled micelles using fluorescence lifetime imaging microscopy. The presence of the DTM label allows the encapsulation of a fluorescent hydrophobic guest (Nile Red) to be monitored by measuring FRET between the DTM (donor) and Nile Red (acceptor). Uptake of the hydrophobic guest dye was found to occur very quickly (< 10 s), while no FRET was observed with a hydrophilic guest (Rhodamine B), indicating that this small molecule is not encapsulated in the micelle core. The use of this simple DTM label can therefore produce fluorescent BCP micelles that can self-report on both their supramolecular structure and the presence or absence of cargo molecules.

ASSOCIATED CONTENT

Supporting Information

The Supporting Information is available free of charge on the ACS Publications website at DOI: 10.1021/acs.macromol.5b02152.

Table S1 and Figures S1–S10 (PDF)

AUTHOR INFORMATION

Corresponding Author

*E-mail: r.k.o-reilly@warwick.ac.uk; Fax +44 024 7652 4112; Tel +44 024 7652 3236 (R.K.O.).

Notes

The authors declare no competing financial interest.

ACKNOWLEDGMENTS

The authors thank Dr Yan Kang for performing TEM analysis. The IAS at the University of Warwick, the ERC (Grant No. 615142), the EPSRC, The Leverhulme Trust, and University of Birmingham are gratefully acknowledged for funding. Some of the spectrometers and SEC equipment used in this research were obtained through Birmingham Science City: Innovative Uses for Advanced Materials in the Modern World (West Midlands Centre for Advanced Materials Project 2), with

support from Advantage West Midlands (AWM) and part funded by the European Regional Development Fund (ERDF).

■ REFERENCES

- (1) Wolfbeis, O. S. *Chem. Soc. Rev.* **2015**, *44*, 4743.
- (2) Canfarotta, F.; Whitcombe, M. J.; Piletsky, S. A. *Biotechnol. Adv.* **2013**, *31*, 1585.
- (3) Chen, M.; Yin, M. *Prog. Polym. Sci.* **2014**, *39*, 365.
- (4) Ruedas-Rama, M. J.; Walters, J. D.; Orte, A.; Hall, E. A. H. *Anal. Chim. Acta* **2012**, *751*, 1.
- (5) Kelley, E. G.; Albert, J. N. L.; Sullivan, M. O.; Epps, T. H., III *Chem. Soc. Rev.* **2013**, *42*, 7057.
- (6) Hu, J.; Liu, S. *Macromolecules* **2010**, *43*, 8315.
- (7) Zhang, P.; Cheatham, A. G.; Lock, L. L.; Li, Y.; Cui, H. *Curr. Opin. Biotechnol.* **2015**, *34*, 171.
- (8) Maiti, C.; Banerjee, R.; Maiti, S.; Dhara, D. *Langmuir* **2015**, *31*, 32.
- (9) Sokolova, V.; Epple, M. *Nanoscale* **2011**, *3*, 1957.
- (10) Robin, M. P.; O'Reilly, R. K. *Polym. Int.* **2015**, *64*, 174.
- (11) Vollrath, A.; Schallon, A.; Pietsch, C.; Schubert, S.; Nomoto, T.; Matsumoto, Y.; Kataoka, K.; Schubert, U. S. *Soft Matter* **2013**, *9*, 99.
- (12) Hudson, Z. M.; Lunn, D. J.; Winnik, M. A.; Manners, I. *Nat. Commun.* **2014**, *5*, 3372.
- (13) Hudson, Z. M.; Boott, C. E.; Robinson, M. E.; Rupar, P. A.; Winnik, M. A.; Manners, I. *Nat. Chem.* **2014**, *6*, 893.
- (14) Chen, J.; Zhang, P.; Fang, G.; Yi, P.; Yu, X.; Li, X.; Zeng, F.; Wu, S. *J. Phys. Chem. B* **2011**, *115*, 3354.
- (15) Wu, C.; Jin, Y.; Schneider, T.; Burnham, D. R.; Smith, P. B.; Chiu, D. T. *Angew. Chem., Int. Ed.* **2010**, *49*, 9436.
- (16) Fuchs, S.; Otto, H.; Jehle, S.; Henklein, P.; Schluter, A. D. *Chem. Commun.* **2005**, 1830.
- (17) Hu, J.; Dai, L.; Liu, S. *Macromolecules* **2011**, *44*, 4699.
- (18) O'Reilly, R. K.; Joralemon, M. J.; Wooley, K. L.; Hawker, C. J. *Chem. Mater.* **2005**, *17*, 5976.
- (19) Webber, S. E. *J. Phys. Chem. B* **1998**, *102*, 2618.
- (20) Major, M. D.; Torkelson, J. M.; Brearley, A. M. *Macromolecules* **1990**, *23*, 1700.
- (21) Cao, T.; Munk, P.; Ramireddy, C.; Tuzar, Z.; Webber, S. E. *Macromolecules* **1991**, *24*, 6300.
- (22) Ylitalo, D. A.; Frank, C. W. *Polymer* **1996**, *37*, 4969.
- (23) Ge, Z.; Liu, S. *Chem. Soc. Rev.* **2013**, *42*, 7289.
- (24) Bo, Q.; Zhao, Y. *Langmuir* **2007**, *23*, 5746.
- (25) Lin, Y.; Zheng, Z.; Hogen-Esch, T. E.; Ling, J.; Shen, Z. *J. Colloid Interface Sci.* **2013**, *390*, 105.
- (26) Noel, A.; Borguet, Y. P.; Wooley, K. L. *ACS Macro Lett.* **2015**, *4*, 645.
- (27) Evans, C. M.; Henderson, K. J.; Saathoff, J. D.; Shull, K. R.; Torkelson, J. M. *Macromolecules* **2013**, *46*, 4131.
- (28) You, S.; Cai, Q.; Mullen, K.; Yang, W.; Yin, M. *Chem. Commun.* **2014**, *50*, 823.
- (29) Yan, Q.; Yuan, J.; Yuan, W.; Zhou, M.; Yin, Y.; Pan, C. *Chem. Commun.* **2008**, 6188.
- (30) Zhou, K.; Wang, Y.; Huang, X.; Luby-Phelps, K.; Sumer, B. D.; Gao, J. *Angew. Chem., Int. Ed.* **2011**, *50*, 6109.
- (31) Zhou, K.; Liu, H.; Zhang, S.; Huang, X.; Wang, Y.; Huang, G.; Sumer, B. D.; Gao, J. *J. Am. Chem. Soc.* **2012**, *134*, 7803.
- (32) Ma, X.; Wang, Y.; Zhao, T.; Li, Y.; Su, L.-C.; Wang, Z.; Huang, G.; Sumer, B. D.; Gao, J. *J. Am. Chem. Soc.* **2014**, *136*, 11085.
- (33) Wang, Y.; Zhou, K.; Huang, G.; Hensley, C.; Huang, X.; Ma, X.; Zhao, T.; Sumer, B. D.; DeBerardinis, R. J.; Gao, J. *Nat. Mater.* **2014**, *13*, 204.
- (34) Liu, T.; Hu, J.; Jin, Z.; Jin, F.; Liu, S. *Adv. Healthcare Mater.* **2013**, *2*, 1576.
- (35) Liu, T.; Liu, S. *Anal. Chem.* **2011**, *83*, 2775.
- (36) Wu, G.; Chen, S.-C.; Liu, C.-L.; Wang, Y.-Z. *ACS Nano* **2015**, *9*, 4649.
- (37) Liu, G.; Hu, J.; Zhang, G.; Liu, S. *Bioconjugate Chem.* **2015**, *26*, 1328.
- (38) Robin, M. P.; Wilson, P.; Mabire, A. B.; Kiviahio, J. K.; Raymond, J. E.; Haddleton, D. M.; O'Reilly, R. K. *J. Am. Chem. Soc.* **2013**, *135*, 2875.
- (39) Mabire, A. B.; Robin, M. P.; Quan, W.-D.; Willcock, H.; Stavros, V. G.; O'Reilly, R. K. *Chem. Commun.* **2015**, *51*, 9733.
- (40) Robin, M. P.; Raymond, J. E.; O'Reilly, R. K. *Mater. Horiz.* **2015**, *2*, 54.
- (41) Mabire, A. B.; Robin, M. P.; Willcock, H.; Pitto-Barry, A.; Kirby, N.; O'Reilly, R. K. *Chem. Commun.* **2014**, *50*, 11492.
- (42) Robin, M. P.; Mabire, A. B.; Damborsky, J. C.; Thom, E. S.; Winzer-Serhan, U. H.; Raymond, J. E.; O'Reilly, R. K. *J. Am. Chem. Soc.* **2013**, *135*, 9518.
- (43) Hua, F.; Jiang, X.; Li, D.; Zhao, B. *J. Polym. Sci., Part A: Polym. Chem.* **2006**, *44*, 2454.
- (44) Robin, M. P.; O'Reilly, R. K. *Chem. Sci.* **2014**, *5*, 2717.
- (45) Nicolai, T.; Brown, W.; Johnsen, R. M.; Stepanek, P. *Macromolecules* **1990**, *23*, 1165.
- (46) Colombani, O.; Ruppel, M.; Burkhardt, M.; Drechsler, M.; Schumacher, M.; Gradzielski, M.; Schweins, R.; Müller, A. H. E. *Macromolecules* **2007**, *40*, 4351.
- (47) Esker, A. R.; Mengel, C.; Wegner, G. *Science* **1998**, *280*, 892.
- (48) Discher, D. E.; Ahmed, F. *Annu. Rev. Biomed. Eng.* **2006**, *8*, 323.
- (49) Patterson, J. P.; Robin, M. P.; Chassenieux, C.; Colombani, O.; O'Reilly, R. K. *Chem. Soc. Rev.* **2014**, *43*, 2412.
- (50) Patterson, J. P.; Sanchez, A. M.; Petzetakis, N.; Smart, T. P.; Epps, T. H., III; Portman, I.; Wilson, N. R.; O'Reilly, R. K. *Soft Matter* **2012**, *8*, 3322.
- (51) Dyson, M. A.; Sanchez, A. M.; Patterson, J. P.; O'Reilly, R. K.; Sloan, J.; Wilson, N. R. *Soft Matter* **2013**, *9*, 3741.
- (52) Hong, Y.; Lam, J. W. Y.; Tang, B. Z. *Chem. Commun.* **2009**, 4332.
- (53) Rajdev, P.; Basak, D.; Ghosh, S. *Macromolecules* **2015**, *48*, 3360.
- (54) Li, C.; Hu, J.; Liu, S. *Soft Matter* **2012**, *8*, 7096.
- (55) Hu, P.; Tirelli, N. *React. Funct. Polym.* **2011**, *71*, 303.
- (56) Elsabahy, M.; Wooley, K. L. *Chem. Soc. Rev.* **2012**, *41*, 2545.
- (57) Moore, B. L.; Lu, A.; Moatsou, D.; O'Reilly, R. K. *Eur. Polym. J.* **2015**, *62*, 380.